Impedance minimization of the CERN Super Proton Synchrotron cavities using the generalized coupled *S*-parameter method

Shahnam Gorgi Zadeh,[1,*] Erion Gjonaj,[2] Thomas Flisgen,[3] Patrick Krämer,[4] Christine Völlinger,[4] and Ursula van Rienen[1,†]

[1]*Institute of General Electrical Engineering, University of Rostock, 18059 Rostock, Germany*
[2]*Institute for Accelerator Science and Electromagnetic Fields, Technische Universität Darmstadt, 64289 Darmstadt, Germany*
[3]*Ferdinand-Braun-Institut gGmbH, Leibniz-Institut für Höchstfrequenztechnik, Berlin, Germany*
[4]*CERN, Geneva, Switzerland*

(Received 27 October 2021; accepted 22 July 2022; published 11 August 2022)

In the context of the Large Hadron Collider (LHC) injector upgrade, components with high contribution to the beam coupling impedance of the injector chain have to be identified and optimized to ensure the delivery of high-intensity proton beams to the LHC. The Super Proton Synchrotron (SPS) is the last accelerator in the LHC injector chain. In the existing design, the longitudinal beam coupling impedance of the SPS cavities limits the increase of the beam intensity in the SPS ring. Since the 200 MHz traveling wave cavities are one of the main contributors to the overall beam coupling budget of the SPS machine, different types of higher-order mode (HOM) couplers are used in the long 33-cell and 44-cell cavities for the damping of various HOMs. The location of the HOM couplers in the cavity, as well as their shape, affects the damping of HOMs. Finding a suitable arrangement of the HOM couplers requires solving a discrete optimization problem. The repetitive calculation of the beam coupling impedance by the conventional time-domain wakefield solvers in the optimization is hindered by the large size of the SPS cavities. The generalized coupled *S*-parameter method is a domain decomposition method for the calculation of the *S* parameters and beam coupling impedance of large structures. In this paper, this method is employed to calculate the beam coupling impedance of the SPS cavities. Then, an optimization method is proposed to find an optimal arrangement of the HOM couplers in the cavities. The article presents the geometrical details of the SPS cavities, a short description of the generalized coupled *S*-parameter method, and a discrete optimization method applied to the SPS cavities.

DOI: 10.1103/PhysRevAccelBeams.25.082001

I. INTRODUCTION

The High-Luminosity Large Hadron Collider (HL-LHC) project implements a major upgrade of the LHC to increase its integrated luminosity by a factor of 10 beyond initial LHC design values [1]. The HL-LHC upgrade is accompanied by the LHC Injector Upgrade (LIU) project [2]. An upgrade of the LHC injectors is mandatory as the injectors were designed in the past for entirely different requirements. The LIU is a challenging task and needs a careful impedance study of all components built into the injectors. A special focus within LIU is on the upgrade of the Super Proton Synchrotron (SPS). SPS is installed in a tunnel of 6.9 km and serves as the final stage of the LHC injector chain [3] before transferring the beam to the LHC. To ensure the planned higher beam intensity of the HL-LHC, the components of the injector chain that limit increasing the beam intensity and brightness have to be identified and optimized. For this reason, intensive studies on the impedance reduction possibilities of the SPS ring are currently being carried out at CERN [4,5].

The interaction of the beam with its surrounding is typically characterized by the concept of beam coupling impedance in the frequency domain (FD). One important contributor to the SPS impedance is the traveling wave cavities operating at the fundamental frequency of 200 MHz. The contribution of the SPS cavities to the overall beam coupling impedance of the SPS ring, along with other major impedance sources, is presented in [4,6]. The upgraded baseline of the SPS cavities includes 33-cell and 44-cell cavities. Beam stability studies have shown that the higher-order modes (HOM) of the SPS cavities around 630 MHz pose a limitation on increasing the beam intensity

*shahnam.zadeh@uni-rostock.de
†Also at Department Life, Light & Matter, University of Rostock, 18051 Rostock, Germany.

since they contribute to the development of longitudinal multibunch instabilities [7]. Although these HOMs are already strongly damped by the existing HOM couplers, a further reduction of the impedance of these modes is required for increasing the stability threshold.

Different approaches have been proposed so far to improve the damping of the modes around 630 MHz such as adding additional HOM couplers of the same design, improvement of the HOM coupler design, and alteration of the structure such that the HOMs are mitigated while the fundamental mode is remaining untouched [8–10]. In addition to the design of the HOM couplers, mainly their location inside the cavity affects their damping performance. On each cell of the SPS cavity, there is an access port that can be used for the installation of HOM couplers. One economical and yet practical possibility for improving the damping of HOMs is changing the arrangement of the couplers in the SPS cavities. Simplified equivalent circuit models of the cavities have been used so far to optimize the HOM couplers and find a suitable location for the couplers in the cavity [11,12]. Following this method, the additional HOM couplers are placed in cells with a large electric field amplitude to mitigate the effect of dangerous modes [8]. However, such an approach lacks accuracy as the beam coupling impedance is not directly considered.

A common approach for calculating the beam coupling impedance is to take the Fourier transform of the wake potential obtained by the excitation of the structure with a bunch of charged particles in the time domain (TD) [13,14]. Several TD wakefield solvers such as ABCI [15], ECHO [16], PBCI [17], and CST STUDIO SUITE® [18] are nowadays available for the impedance calculation of complex geometries. Most of these solvers use the finite integration technique (FIT) [19,20] to discretize Maxwell's equations. The time-step size in explicit TD approaches is typically limited by the Courant-Friedrichs-Lewy (CFL) criterion [21]. At a given sampling rate in TD, the frequency resolution is limited by the length of the sampling sequence, and thus a very long wake length is required to resolve sharp impedance peaks. Another approach is to calculate the beam coupling impedance directly in FD by including the excitation term (here beam current) in the time-harmonic Maxwell's equation. One advantage of this method is that the beam coupling impedance can be arbitrarily sampled around the frequency of interest.

Due to the large size of the SPS cavities, the calculation of the beam coupling impedance either in TD or FD is computationally very expensive, especially for the optimization where many objective function evaluations are required. In the last two decades, several domain-decomposition methods have been proposed for the calculation of the radio-frequency (rf) properties of a large structure. The scattering matrix of a multiport complex structure could be constructed based on the scattering matrices of its segments using the coupled *S*-parameter calculation method (CSC) [22–24]. The state-space concatenation (SSC) method combines the model-order reduction technique with the domain-decomposition method to calculate the eigenmodes of a large structure [25–27]. A recently proposed generalized coupled *S*-parameter method $\mathrm{CSC}^{\mathrm{BEAM}}$ generalizes the CSC method by considering the beam current as an additional port in the scattering matrix [28]. In this method, the beam coupling impedance, along with the S-parameters, is sampled at arbitrary discrete frequencies.

This paper presents an application of the $\mathrm{CSC}^{\mathrm{BEAM}}$ method to find an optimum arrangement of the HOM couplers of the SPS cavities. With this approach, sampling the generalized scattering matrices at frequencies with relevant HOMs and treating identical cells of the SPS cavities only once significantly reduce the computational effort. The goal of the optimization is to decrease the impedance peak around 630 MHz by rearranging the HOM couplers, and if possible, reduce the number of HOM couplers without deteriorating their overall damping performance.

The structure of this paper is as follows: Section II presents an overview of the existing design of the SPS cavity and its HOM couplers. In Sec. III, the $\mathrm{CSC}^{\mathrm{BEAM}}$ is revised. The adopted optimization approach is described in Sec. IV. In Sec. V, the simulation setup and the results of the optimization for the 33-cell and 44-cell cavities are presented. Section VI concludes this paper.

II. SPS TRAVELING WAVE CAVITIES

For manufacturing and practical considerations, the traveling wave cavities (TWCs) are built by concatenated sections each consisting of 11 cells as shown in Fig. 1(b). Two four-section (44-cell) and two five-section (55-cell) cavities were in operation in the SPS until 2018. A picture of the five-section cavity in the SPS tunnel is shown in Fig. 1(c). After the Long Shutdown 2 (LS2), the cavities are rearranged in the context of an rf upgrade so that now six TWCs are installed. Today, there are four three-section (33-cell) and two four-section (44-cell) cavities using two additional sections [29]. Each unit cell of the traveling wave accelerating cavity of the SPS is composed of a drift tube connected to the outer cylindrical structure by horizontal bars [see Fig. 1(a)]. The TWC operates at the frequency of 200.222 MHz with a $\pi/2$ phase advance between the adjacent cells [30]. The length and diameter of each unit cell of the cavity are 0.374 and 0.75 m, respectively.

Several types of HOM couplers are used in the SPS cavity for the damping of various HOM passbands. Beam dynamic studies have shown that the modes at around 630 MHz are one of the impedance sources that can drive beam instability at the high beam intensities required in the future [4,6]. Therefore, further reduction of the longitudinal beam coupling impedance at 630 MHz is required. There is

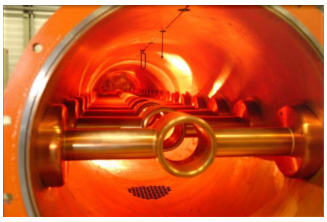

(a) Inside view of the SPS cavity (Image: ©CERN)

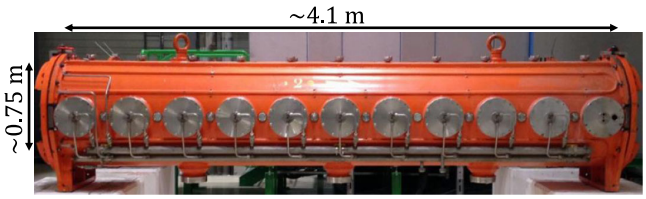

(b) One section of the SPS cavity [31]

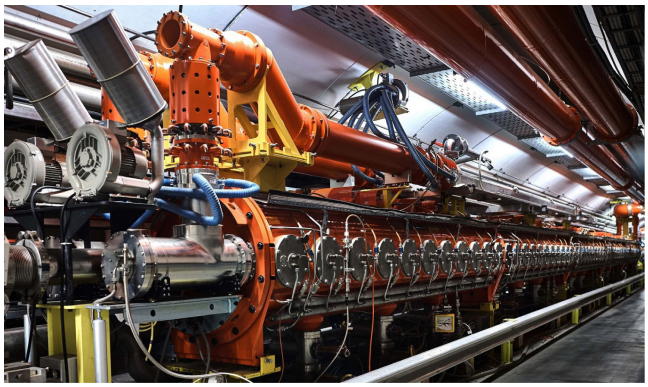

(c) Five-section cavity

FIG. 1. An inside view of the SPS cavity is shown in (a) [[9] p. 44]. One section of the SPS cavity is composed of 11 cells (b). An access port on top of each cell allows for the installation of the HOM couplers. A five-section cavity is shown in (c).

an access port on top of each cell through which the HOM couplers can be installed. Figure 2 shows some of the HOM couplers that are being used in the SPS cavity. Each middle cell can be either left without a HOM coupler [Fig. 2(a)] or it can be equipped with one of the three different HOM coupler designs [Figs. 2(b)–2(d)]. The coaxial coupler shown in Fig. 2(f) is mainly designed for the damping of HOMs at 630 MHz. An optimization study for this coupler has been carried out during the last years [9]. It was demonstrated that the damping of the modes at around 630 MHz can be improved by terminating the HOM couplers with different impedance loads than the previously used 50 Ω. In particular, to obtain a maximum reduction of shunt impedance of the most critical modes, a load impedance of approximately 25 Ω in the reference plane gives the best compromise. This is implemented by replacing the 50 Ω load with a complex load impedance built of a defined coaxial line length with 25 Ω termination while the pickup part of the HOM coupler can stay unmodified. In this paper, we will refer to this HOM

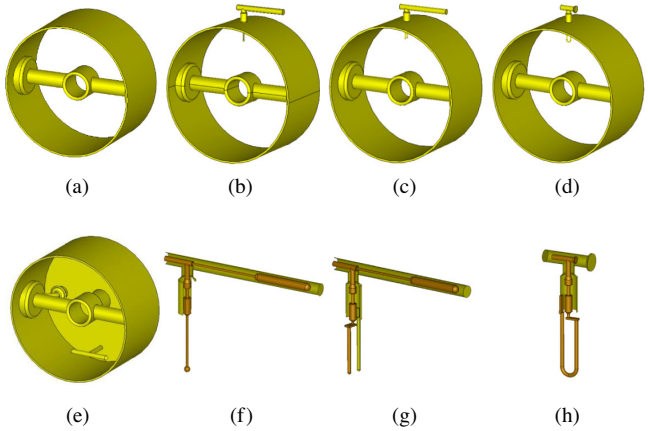

FIG. 2. A simulation model of the middle cell without a HOM coupler (a), with different types of HOM couplers (b–d), and the end cell (e). Note that each cell also contains a drift tube supported by stems which are mounted on pedestals. (f) The probe-type HOM coupler with antenna pickups designed to damp the HOMs of the passband at 630 MHz. (g) HOM coupler with parallel line pickups (also referred to as fork-type coupler) designed for the damping of 630 MHz modes in the four-section cavity. (h) Loop-type HOM coupler designed for the damping of the transversal modes at around 938 MHz. The simulation models are created with CST STUDIO SUITE®.

coupler as the probe-type coupler. Eight fork-type couplers with parallel line pickups are also designed and installed in the four-section cavities to improve the damping of 630 MHz modes [12]. A termination load of 50 Ω is used in the fork-type couplers. This coupler is shown in Fig. 2(g). Loop-type couplers, shown in Fig. 2(h), are used to damp the modes with high transverse impedance at 938 MHz. The end cell contains the fundamental power coupler (FPC) connected to the pedestal of the drift tube and also dipole-like antennas designed for the damping of transverse modes at 460 MHz [see Fig. 2(e)]. In this paper, we have used a simplified model of the end cell that does not include the FPC and the 460-MHz couplers. This simplification is justified since these two types of couplers have only a minor influence on the impedance at around 630 MHz.

Figure 3 shows the proposed HOM damping configuration after LS2. The present design considers 16 probe-type couplers, six loop-type couplers, and eight fork-type couplers for the 44-cell cavity, and 18 probe-type and four loop-type couplers for the 33-cell cavity. Four probe-type couplers were initially considered for each section of the cavity, i.e., 12 probe-type couplers for the 33-cell cavity. To further damp the modes with high geometric shunt impedance (R/Q) around 630 MHz, six additional probe couplers are added to the HOM damping configuration of the 33-cell cavity. The positions of these additional couplers are shown as underlined red numbers in Fig. 3(a) and are placed in the cells that have a high value of the electric field for some HOMs with a large value of R/Q [8]. Because of the large size of the cavities, finding an optimum arrangement of the

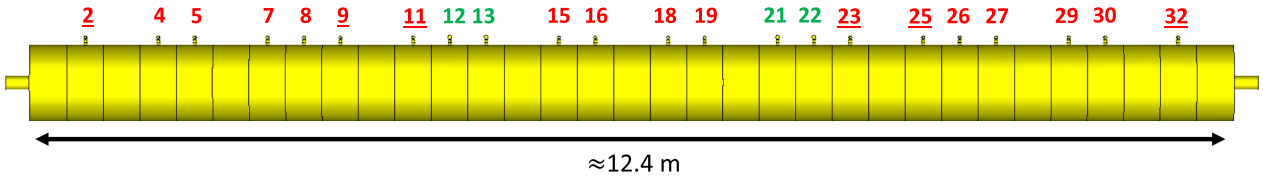

(a) 33-cell cavity

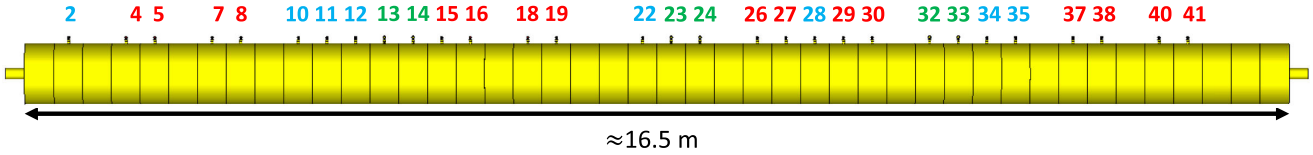

(b) 44-cell cavity

FIG. 3. The simulation model of the 33-cell (a) and 44-cell (b) cavity shows the existing HOM damping schemes. The present locations of the loop-type couplers are shown by green numbers, the fork-type couplers by blue numbers, and the probe-type couplers by red numbers. In order to improve the damping of modes at 630 MHz, six probe-type couplers are proposed to be added to the existing damping design of the 33-cell cavity after LS2 (shown by underlined red numbers).

HOM couplers with the TD wakefield solvers is very time consuming. As an example, a single TD simulation of the 44-cell cavity with 51×10^6 hexahedral elements and 600 m wakelength with CST STUDIO SUITE® takes around 108 h on a PC with Intel(R) Xeon(R) Gold 6246 CPU 3.3 GHz and 256 GB RAM. For this reason, the CSC$^{\mathrm{BEAM}}$ method will be used in the following sections to find an optimum configuration of the HOM couplers.

III. GENERALIZED COUPLED *S*-PARAMETER METHOD

To determine the beam-coupling impedances of the SPS cavities, shown, e.g., in Fig. 3, the SPS cavities are decomposed into individual segments. The resulting segments are depicted in Fig. 2. Each segment is indexed by r, as sketched in Fig. 4(a). At the interface planes between the individual segments, the 2D Helmholtz equation is solved on the respective cross sections (marked in red in Fig. 4), so that a finite set of orthogonal waveguide modes is available to expand the electric and magnetic fields on these cross sections. Following Fig. 4(b), the left and right port planes are indexed by $p = 1$ and $p = 2$, respectively. On the left port plane, n orthogonal modes are considered and on the right port plane m modes. Incident and scattered wave amplitudes $\underline{a}_{r,p,m}$ and $\underline{b}_{r,p,m}$ correspond to each of the modes. In addition, for each segment, a beam current $\underline{i}_r$ and the induced beam voltage $\underline{v}_r$ are considered. For further details on these quantities, see Eqs. (4) and (5) in [28].

Each segment is described by a generalized scattering matrix

$$\begin{pmatrix} \underline{\mathbf{s}}_{11} & \underline{\mathbf{s}}_{12} & \underline{\mathbf{k}}_1 \\ \underline{\mathbf{s}}_{21} & \underline{\mathbf{s}}_{22} & \underline{\mathbf{k}}_2 \\ \underline{\mathbf{h}}_1 & \underline{\mathbf{h}}_2 & \underline{z} \end{pmatrix} \begin{pmatrix} \underline{\mathbf{a}}_1 \\ \underline{\mathbf{a}}_2 \\ \underline{i} \end{pmatrix} = \begin{pmatrix} \underline{\mathbf{b}}_1 \\ \underline{\mathbf{b}}_2 \\ \underline{v} \end{pmatrix}, \tag{1}$$

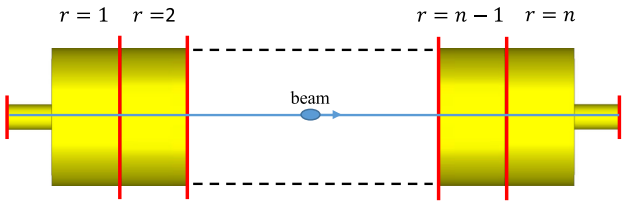

(a) Decompose the structure.

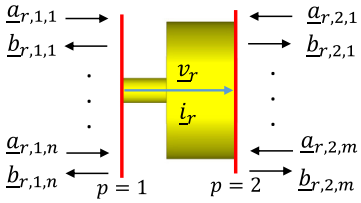

(b) Create the generalized scattering matrix for each segment.

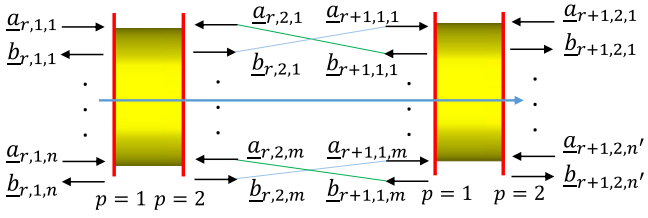

(c) Concatenate the segments.

FIG. 4. Steps of the CSC$^{\mathrm{BEAM}}$ method. The geometry is first decomposed into nonoverlapping segments (a). Each segment is then terminated by a waveguide port, shown by red vertical lines, and the generalized scattering matrix for each segment is created (b). The amplitude of the incident and reflected wave of mode m of port p of segment r is denoted by $\underline{a}_{r,p,m}$ and $\underline{b}_{r,p,m}$, respectively. Using the continuity of the electromagnetic field at the intersections, the segments are concatenated using algebraic equations (c).

where $\underline{\mathbf{a}}_1$, $\underline{\mathbf{a}}_2$, $\underline{\mathbf{b}}_1$, $\underline{\mathbf{b}}_2$ hold the incident and scattered wave amplitudes at the left and the right ports, $\underline{i}$ and $\underline{v}$ are the beam current and voltage, $\underline{\mathbf{s}}_{ij}$ is the commonly known scattering matrix block for a two-port network, $\underline{\mathbf{k}}_i$ is the coupling factor between beam current and scattered wave amplitudes at both ports, and $\underline{z}$ is the commonly known beam coupling impedance. All quantities are complex-valued and frequency dependent. The index r is omitted for better readability in Eq. (1).

In the next step, the generalized scattering matrices [Eq. (1)] of all segments are concatenated. The continuity of field components across the segments is accomplished by equating scattered wave amplitudes with the respective incident wave amplitudes of the adjacent segments. For the example shown in Fig. 4(c), this results in

$$\begin{aligned} \underline{b}_{r+1,1,1} &= \underline{a}_{r,2,1}, \quad \underline{b}_{r,2,1} = \underline{a}_{r+1,1,1}, \\ &\vdots \qquad\qquad \vdots \\ \underline{b}_{r+1,1,m} &= \underline{a}_{r,2,m}, \quad \underline{b}_{r,2,m} = \underline{a}_{r+1,1,m}. \end{aligned} \tag{2}$$

According to the procedure in [28], continuity conditions for the waveguide modes are used to eliminate intermediate scattered amplitudes at the interface between inner segments. This results in a global scattering matrix for the overall structure. In particular, this procedure allows determining the total beam impedance of the structure. Details of how the procedure is implemented are found in [28].

IV. OPTIMIZATION METHOD

An optimum arrangement of the probe-type and fork-type couplers, which are designed for the damping of modes at 630 MHz, has to be determined using the CSC$^{\mathrm{BEAM}}$ method. In the 33-cell cavity, 18 probe-type couplers have to be placed in 27 cells without a coupler. The location of the loop-type couplers is not changed in this study; however, they are part of the geometry as they impact the overall field distribution. Consequently, cells with loop-type couplers and also end cells cannot be considered in the optimization. The total number of combinations is

$$C(27,18) = \frac{27!}{18!(27-18)!} = 4686\,825. \tag{3}$$

Similarly, the total possible combinations for placing 16 probe-type couplers in 28 empty cells and 8 fork-type couplers in 20 empty cells of the 44-cell cavity are 30421755 and 125970, respectively. The space of the possible solutions is too large to evaluate all arrangements directly. Thus, a combinatorial optimization problem has to be solved to find an optimal arrangement within a reasonable amount of computing time.

A two-step heuristic optimization method is used in this paper as given in Table I. Step 1 is based on the nearest neighbor optimization method [32]. This algorithm can be applied in two ways in our case. Start from zero HOM couplers and add them one by one [step 1(a)] or start from HOM couplers on all cells and remove them one by one [step 1(b)]. The results of these two approaches are then compared and the configuration that yields a smaller longitudinal impedance peak for a specific number of HOM couplers is selected.

TABLE I. Optimization algorithm steps.

1. Perform steps 1(a) and 1(b) and select the arrangement that yields a smaller real part of the longitudinal impedance with N_c couplers
   (a) Start with zero HOM couplers:
      (i) Add a HOM coupler one at a time to the empty middle cells and calculate the impedance for each case
      (ii) Keep the coupler on the cell that maximally decreases the impedance peak and go to step i
   (b) Put a HOM coupler on all empty middle cells:
      (i) Remove the HOM couplers one at a time and calculate the impedance for each case
      (ii) Discard the HOM coupler with the least influence on the impedance peak and go to step i
2. Evaluate all possible combinations that result from repositioning one HOM coupler from a cell with coupler to an empty cell. If the impedance peak is reduced, update the configuration and repeat the procedure.

The nearest neighbor optimization method does not always yield the best solution; however, its implementation requires a reasonable number of steps. In addition to optimizing the coupler configurations, this method also allows us to obtain the influence of the coupler number on the impedance peak. After reaching the desired number of couplers, step 2 is used to improve the result. In this step, all possible combinations that arise from repositioning only one HOM coupler to a cell without a coupler are studied, and the configuration is updated if the impedance peak is reduced. This step assures that there is no better solution in the neighborhood of the found configuration that can be obtained by changing the location of one HOM coupler. The optimization procedure is automated in MATLAB [33]. All generalized matrices of the segments are first loaded into MATLAB; then, steps 1(a) and 1(b) of the optimization algorithm are executed in separate runs. Next, the configuration with a smaller beam coupling impedance peak is selected as input for step 2 of the optimization algorithm.

V. RESULTS

The 44-cell and 33-cell cavities are comprised of six different types of segments, i.e., two end cells; a cell without a HOM coupler; and cells equipped with one of the three existing couplers, i.e., probe-type, loop-type, and fork-type HOM coupler. The generalized scattering matrices for each segment have to be created separately.

Thus, only six simulation runs for the generalized scattering matrices [Eq. (1)] of these segments are needed before the optimization procedure is applied. A special hybrid type of mesh comprised of hexahedral, tetrahedral, and pyramidal elements is used for the discretization of the segments profiting from the advantages of different mesh types. Hexahedral elements are used to discretize the region around the beam. This type of structured grid around the beam results in a noise-free calculation of the beam coupling impedance on the longitudinal axis [28,34]. An unstructured grid of tetrahedral elements is used to capture all the details of the geometry. Hexahedral elements are connected to the tetrahedrons by a layer of pyramidal elements. A different mesh setting at the cross section between segments can create a small discrepancy between the 2D field in adjacent segments and generate numerical errors. To avoid this error, employ the same order of 2D port modes in the decomposition planes and thus simplify the concatenation scheme in the CSC$^{\mathrm{BEAM}}$ method, an identical 2D mesh is used in all segments at the interface planes. Figure 5 shows an example of the mesh structure of the cell with a loop-type HOM coupler. The meshes for all segments were generated using the SALOME software [35].

Second-order mesh elements are considered in the finite element method (FEM) formulation. The generalized scattering matrices are computed from 615 to 637 MHz with a step size of 0.1 MHz. It took around 4 days to create the generalized scattering matrices of each segment type using a FEM-based frequency domain impedance solver with an in-house simulation code. These calculations include 221 frequency samples and a maximum of 300 waveguide scattering amplitudes (150 modes at each interface) for each of the considered segments. The single frequency calculations are independent of each other, different from the TD approach. Thus, theoretically, each of the frequency samples could be also calculated in a separate run which would reduce simulation time drastically. Since the calculation of generalized scattering matrices is performed only once, however, the simulation time during this step is less critical for the optimization procedure. Considering that a single full simulation of the 44-cell cavity using CST STUDIO SUITE®'s wakefield solver takes about the same amount of time, evaluating thousands of configurations with the wakefield simulation of the full model is not feasible. In contrast, once the generalized matrices are created, the method presented here enables evaluating each configuration within minutes.

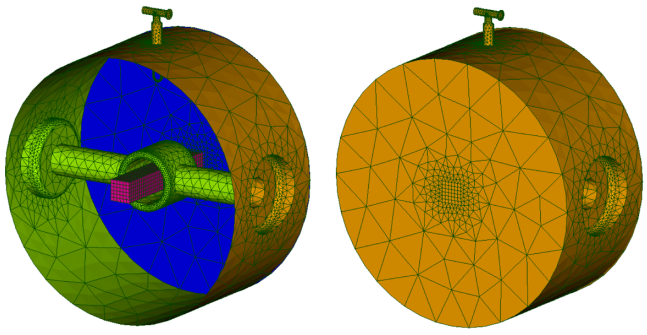

FIG. 5. Mesh structure for impedance calculations using a hybrid mesh comprised of tetrahedral, hexahedral, and pyramidal mesh cells.

Once the scattering matrices are available, the CSC$^{\mathrm{BEAM}}$ approach can be applied to obtain the total impedance. Thereby, the most critical parameter is the number of coupling waveguide modes (wave amplitudes) that are considered in the concatenation procedure. Generally, all modes with a cutoff frequency below the frequency of interest and some evanescent modes have to be taken into account. A higher number of 2D port modes increases the accuracy at the cost of a higher simulation time. Thus, a compromise between the number of 2D port modes and the simulation time has to be determined. Figure 6(a) shows a convergence study for the calculation of the longitudinal impedance, and Fig. 6(b) displays the required simulation time for the concatenation of segments in each case.

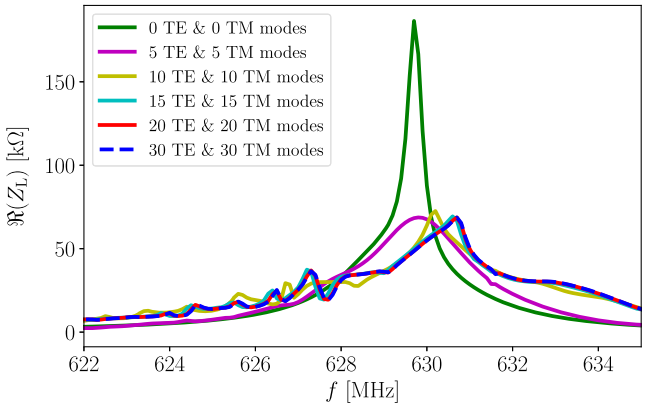

(a) Real part of the longitudinal impedance

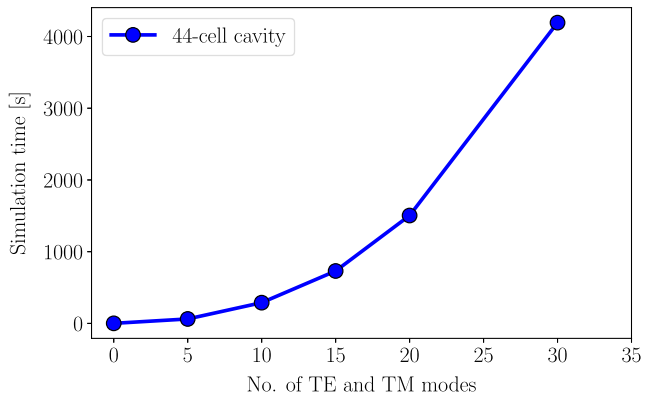

(b) Required simulation time for the concatenation

FIG. 6. The real part of the beam impedance of the 44-cell cavity considers different numbers of port modes at the intersections (a). The required simulation time for the concatenation of segments for each case is shown in (b).

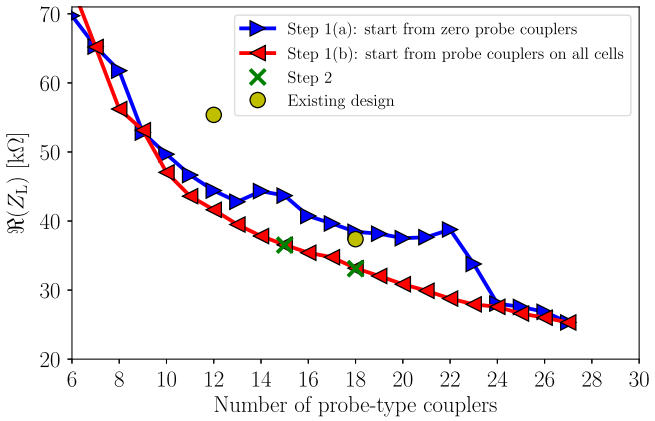

FIG. 7. The peak value of the longitudinal impedance of the 33-cell cavity at around 630 MHz for a different number of probe-type HOM couplers. The yellow markers indicate the peak impedance of the configurations shown in Fig. 3(a).

The simulation time required for the computation of the generalized scattering matrices is not shown in Fig. 6(b). Once the generalized matrices are created, different concatenation setups can be quickly analyzed in the post-processing. Figure 6(b) corresponds to the simulation time for a serial frequency sweep. Again, since the frequency calculations are independent, the simulation time that is shown in Fig. 6(b) can be reduced in a parallelized code. However, the trend between the concatenation simulation time and the number of port modes remains the same.

Increasing the number of transverse electric (TE) and transverse magnetic (TM) modes at the decomposition planes to a number above 20 does not have a tangible effect on the beam coupling impedance, while it substantially increases the simulation time. Therefore, as a compromise

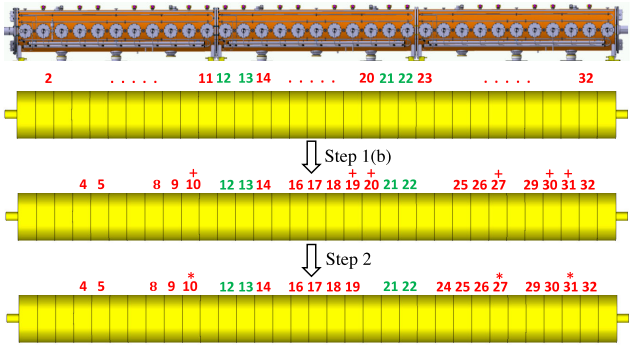

FIG. 8. Progression of the arrangement of the HOM couplers of the 33-cell cavity after each step of the optimization. The green and red numbers show the location of the loop- and probe-type couplers, respectively. In step 1(b), the number of probe-type couplers is reduced one by one starting from couplers on all empty middle cells. The $*$ and $+$ symbols show the HOM couplers that can be removed to optimally decrease the number of probe-type couplers from 18 to 15 and 12 in step 1(b) and step 2, respectively.

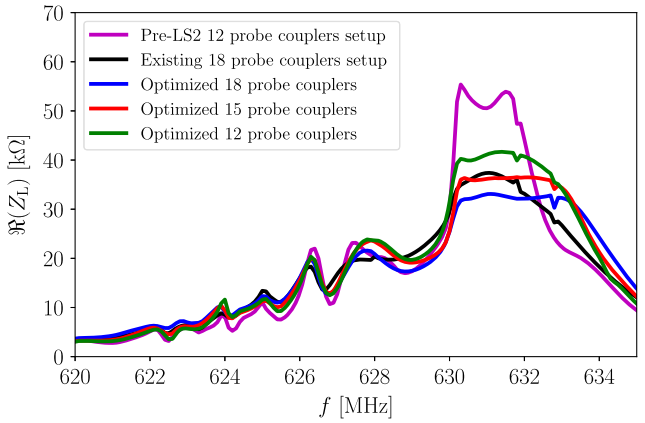

FIG. 9. Real part of the longitudinal impedance of the 33-cell cavity of the existing arrangements shown in Fig. 3(a) and the optimized arrangements shown in Fig. 8. Four probe-type couplers, as arranged before LS2, are considered for each section in the pre-LS2 12-probe couplers setup [see Fig. 3(a)].

20 TE and 20 TM port modes are considered on the decomposition planes. That results in a total of 80 wave amplitude entries in the scattering matrix of each individual segment. Impedance results with CSC$^{\text{BEAM}}$ can slightly differ from those obtained by other codes (e.g., CST STUDIO SUITE®) due to the differences in the mesh, wake integration method, wakelength (in TD), concatenation error, etc. Therefore, CSC$^{\text{BEAM}}$ is used here only to optimize the configuration. Final impedance calculations should be verified with another code.

A. Three-section cavity optimization

The optimization is first carried out on the 33-cell cavity to find an optimum arrangement of the probe-type couplers. Figure 7 shows the peak value of the real part of the longitudinal impedance in the considered frequency range

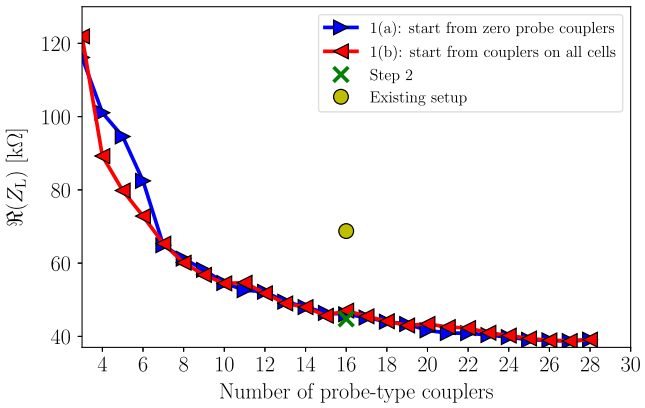

FIG. 10. Peak value of the longitudinal impedance of the 44-cell cavity at around 630 MHz using a different number of probe-type couplers. The yellow marker shows the peak impedance of the existing configuration shown in Fig. 3(b).

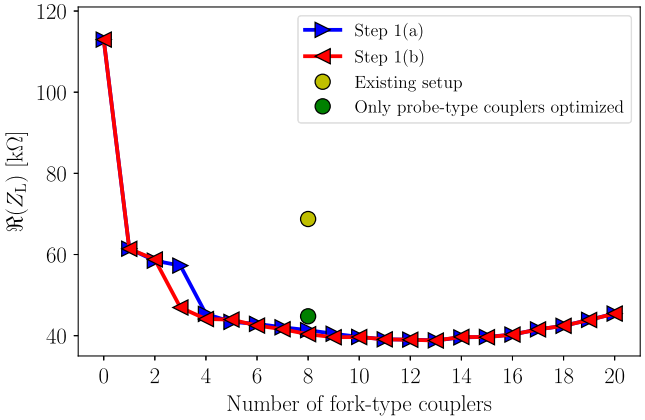

FIG. 11. Impedance peak of the 44-cell cavity after each step of the optimization applied on the fork-type couplers. The yellow marker shows the peak impedance of the existing configuration shown in Fig. 3(b), and the green marker corresponds to the impedance peak obtained by only optimizing the probe-type couplers (shown in Fig. 10).

after each step of Algorithm 1. The nearest neighbor approach (step 1) follows different paths depending on the starting condition. Step 1(b), starting with probe-type couplers on all empty cells and decreasing them stepwise, results in a smaller impedance peak for 18 HOM couplers compared to step 1(a). This is probably because the resolution of the impedance (0.1 MHz) is not sufficient to accurately resolve the high impedance peaks when only a few HOM couplers are used. Therefore, the first few HOM couplers that are added in step 1(a) may not be the optimum ones. While in step 1(b), the starting point yields a low impedance peak, and thus a frequency resolution of 0.1 MHz is sufficient to detect the HOM coupler with the least influence on the impedance peak in the first few steps.

Figure 8 shows the arrangement of the HOM couplers after step 1(b). For 18 HOM couplers, the total number of simulations required in steps 1(a) and 1(b) is 333 and 207, respectively. Step 2 is then applied to the optimum configuration found in step 1(b). Step 2 slightly improves the result as shown in Fig. 7. This step, however, assures that there is no good solution in the neighborhood of the obtained solution. In step 2, the HOM coupler in cell 20 is moved to cell 24. The number of simulations carried out in step 2 is 260. The final configuration after step 2 is shown in Fig. 8.

A plot of the real part of the longitudinal impedance for the existing arrangements, given in Fig. 3(a), and the proposed arrangements, given in Fig. 8, are shown in Fig. 9. Compared to the initial designs, the impedance peak of the 33-cell cavity could be reduced by 25% using 12 probe-type couplers and by 11% using 18 couplers. A flat peak of the impedance curve at 630 MHz indicates that the modes are heavily damped with the found configuration. Due to the large number of HOM couplers used in the 18 probe-type coupler setup, the damping performance cannot be significantly improved by changing the location of the HOM couplers. Alternatively, one can use a smaller number of probe-type couplers, e.g., only 15 couplers, and

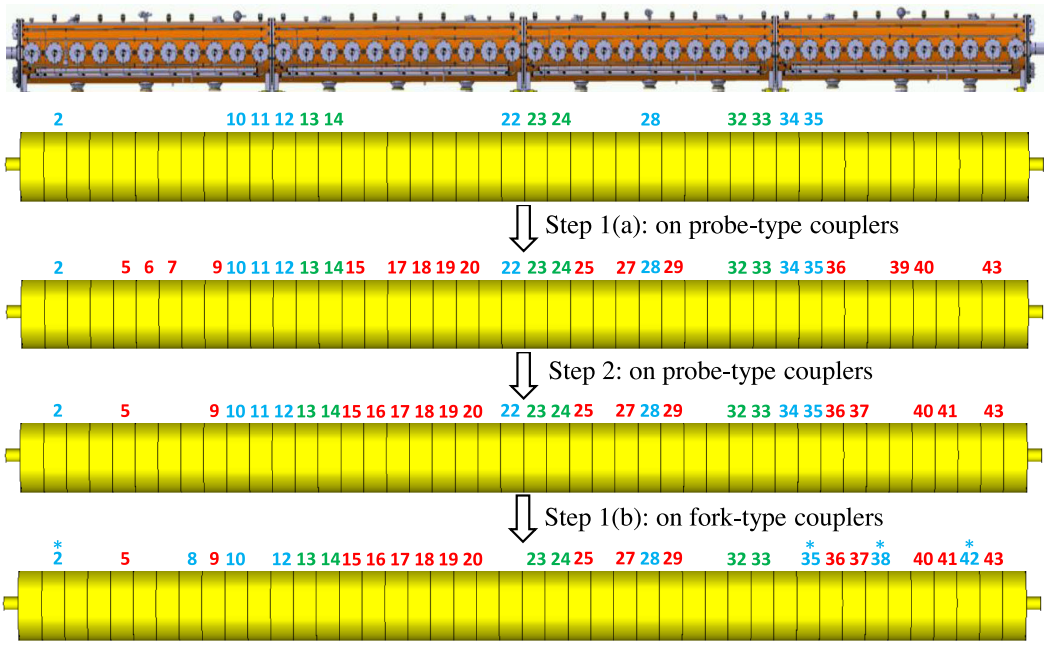

FIG. 12. Progression of the arrangement of the HOM couplers of the 44-cell cavity after each step of the optimization. The green, blue, and red numbers show the location of the loop-, fork-, and probe-type couplers, respectively. The asterisks in the last step show the location of couplers that can be removed to optimally decrease the number of fork-type couplers to 4.

obtain a similar impedance spectrum as the existing setup (see Fig. 9).

B. Four-section optimization

A similar approach is used to find an optimum configuration of the probe- and fork-type couplers in the 44-cell cavity. In the first step, an optimum arrangement for the 16 couplers is found while keeping the location of the fork-type and loop-type couplers fixed. As shown in Fig. 10, the impedance peak of step 1(a) at 16 couplers is marginally below the outcome of step 1(b), and step 2 slightly improves that result. The arrangement of the HOM couplers is shown in Fig. 12. The total number of simulations in step 1(a), step 1(b), and step 2 were 328, 270, and 592, respectively.

In the next step, the locations of the probe-type couplers are fixed and the arrangement of the eight fork-type couplers is optimized. For this purpose, steps 1(a) and 1(b) of the optimization algorithm given in Table 1 are applied to the fork-type coupler. Since the position of the probe-type couplers is fixed, the fork couplers may only be placed on the remaining empty center cells. Figure 11 shows the impedance peak after each step of the optimization. Using more than eight fork-type couplers cannot significantly improve the impedance peak, and even going above 13 fork-type couplers deteriorates the impedance peak. By optimizing the location of the fork-type couplers, the impedance peak is decreased further by around 10%. A similar damping performance as eight fork-type couplers could also be obtained by using four fork-type couplers. The total number of simulations carried out in step 1(a) and step 1(b) are 132 and 174, respectively. The impedance could not be reduced further in step 2. The final proposed arrangement of the HOM couplers of the 44-cell cavity is shown in Fig. 12.

Figure 13 shows the real part of the longitudinal impedance for the existing arrangement shown in Fig. 3(b) and the proposed arrangement given in Fig. 12. Compared to the existing setup, the impedance peak of the 44-cell cavity could be reduced by about 41% just by rearranging the HOM couplers.

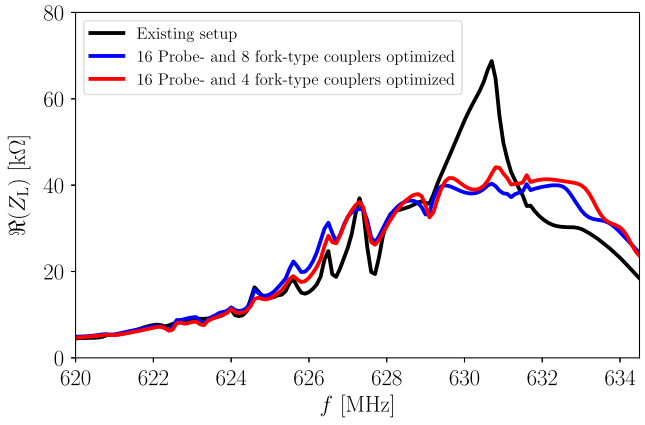

FIG. 13. Real part of the longitudinal impedance of the 44-cell cavity of the existing arrangement shown in Fig. 3(b) and the optimized arrangement shown in Fig. 12.

VI. CONCLUSION

This paper presented the application of the CSC$^{\mathrm{BEAM}}$ method to find an optimized arrangement of the HOM couplers of the 33-cell and 44-cell SPS traveling wave cavities. The focus of the optimization was to minimize the longitudinal impedance at around 630 MHz. In the CSC$^{\mathrm{BEAM}}$ method, the beam coupling impedance is directly calculated in the frequency domain, and once the generalized scattering matrices of segments are created, many different HOM coupler configurations can be evaluated in a very short time. One advantage of this method over the TD approach, in this application, is that the beam coupling impedance can be sampled directly around the desired frequency range. The optimization targets the number and the positioning of the different HOM coupler types in the individual cells of the large traveling wave structure.

It was shown that changing the location of the 12 and 18 probe-type couplers in the 33-cell cavity can reduce the impedance peak of the 630-MHz band by about 25% and 11%, respectively, in comparison to the initial setup. It was further demonstrated that with the use of 15 probe-type couplers, a similar damping performance for the peak value can be reached as with the initial 18 probe-type couplers setup in the 33-cell cavity. In this case, a redistribution of the impedance also takes place leading to the larger impedance at higher frequencies. It must, therefore, still be determined with beam dynamics studies if the moderate reduction in peak impedance is actually desirable and what the final HOM coupler configuration should be.

Contrary to this, changing the arrangement of the probe- and fork-type couplers in the 44-cell cavity provides indeed a reduction of the impedance peak by about 41%. In addition, the number of fork-type couplers that are required in the 44-cell cavity can be reduced from 8 to 4 and yet a similar damping performance can be obtained, again with a slight redistribution of the overall impedance toward higher frequencies. In particular, the reduction of the number of fork couplers could prove advantageous since the insertion of each HOM coupler also causes a slight shift of the frequency of the accelerating mode of the cavity to lower values—a known and undesired side effect of any HOM damping setup.

ACKNOWLEDGMENTS

This work has been supported by the German Federal Ministry for Research and Education BMBF under Contract No. 05H18HRRB1.

[1] G. Apollinari, I. Béjar Alonso, O. Brüning, M. Lamont, and L. Rossi, High-Luminosity Large Hadron Collider (HL-LHC): Preliminary Design Report, Report No. CERN-2015-005, CERN Yellow Reports: Monographs (CERN, Geneva, 2015).

[2] H. Damerau, A. Funken, R. Garoby, S. Gilardoni, B. Goddard, K. Hanke, A. Lombardi, D. Manglunki, M. Meddahi, B. Mikulec, G. Rumolo, E. Shaposhnikova, M. Vretenar, and J. Coupard, LHC Injectors Upgrade, Technical Design Report, CERN Technical Report No. CERN-ACC-2014-0337, 2014.

[3] K. Schindl, The injector chain for the LHC, revised version, CERN Report No. CERN-PS-99-018-DI, 1999.

[4] E. Shaposhnikova, T. Argyropoulos, T. Bohl, P. Cruikshank, B. Goddard, T. Kaltenbacher, A. Lasheen, J. Perez Espinos, J. Repond, B. Salvant, and C. Vollinger, Removing known SPS intensity limitations for high luminosity LHC goals, in *Proceedings of the 7th International Particle Accelerator Conference, IPAC-2016, Busan, Korea* (JACoW, Geneva, Switzerland, 2016), MOPOY058.

[5] A. Farricker and C. Vollinger, Impedance reduction in the CERN SPS through element layout optimisation, in *Proceedings of the 10th International Particle Accelerator Conference, IPAC-2019, Melbourne, Australia* (JACoW Publishing, Geneva, Switzerland, 2019), MOPGW077.

[6] A. Lasheen, T. Argyropoulos, J. Repond, and E. Shaposhnikova, Effect of the various impedances on longitudinal beam stability in the CERN SPS, in *Proceedings of the 7th International Particle Accelerator Conference, IPAC-2016, Busan, Korea* (JACoW, Geneva, Switzerland, 2016), pp. 1666–1669.

[7] J. Repond, Possible mitigations of longitudinal intensity limitations for HL-LHC beam in the CERN SPS 2019, École polytechnique fédérale de Lausanne (EPFL), Report No. CERN-THESIS-2019-173, 2019.

[8] P. Kramer and C. Vollinger, HOM-mitigation for future SPS 33-cell 200 MHz accelerating structures, in *Proceedings of the 13th International Computational Accelerator Physics Conference, ICAP2018, Key West, FL, 2018* (JACoW, Geneva, Switzerland, 2019), SAPAG04.

[9] P. Krämer, Studies of higher order mode couplers for the upgraded travelling wave acceleration system in the CERN SPS, Ph.D. thesis, Rheinisch-Westfälischen Technischen Hochschule Aachen, 2020.

[10] N. Nasresfahani, HOM damping in accelerating cavities with large number of cells: Application to 44-Cell TWCs of CERN SPS, in *Proceedings of the ICFA Mini Workshop on Higher Order Modes in Superconducting Cavities, HOMSC2018, Cornell University* (2018), https://indico.classe.cornell.edu/event/185/contributions/558/.

[11] N. Nasr Esfahani, P. Kramer, and C. Vollinger, Equivalent circuit modelling of travelling wave accelerating structures and its applications, in *Proceedings of the 47th European Microwave Conference, Nuremberg, Germany* (2017), pp. 572–575, 10.23919/EuMC.2017.8230912.

[12] N. Nasresfahani, Travelling wave structures; *Focus on an approach for HOM damping of 44-cell travelling wave cavities of SPS*, (CERN, Geneva, Switzerland, 2019), https://indico.cern.ch/event/843868/.

[13] B. Zotter and S. Kheifets, *Impedances and Wakes in High Energy Particle Accelerators* (World Scientific, Singapore, 1998).

[14] T. Weiland and R. Wanzenberg, Wake fields and impedances, DESY Report No. DESY M-91-06, 1991.

[15] Y. Chin, Advances and Applications of ABCI, in *Proceedings of the 15th Particle Accelerator Conference, PAC-1993, Washington, DC, 1993* (IEEE, New York, 1993).

[16] https://echo4d.de/.

[17] E. Gjonaj, T. Lau, T. Weiland, and R. Wanzenberg, Computation of short range wake fields with PBCI, ICFA Beam Dyn. Newsl. **45**, 38 (2008).

[18] Computer Simulation Technology, CST Studio Suite, https://www.3ds.com/products-services/simulia/products/cst-studio-suite/.

[19] T. Weiland, A discretization model for the solution of Maxwell's equations for six-component fields, AEU Int. J. Electron. Commun. **31**, 116 (1977).

[20] T. Weiland, Time domain electromagnetic field computation with finite difference methods, Int. J. Numer. Model. **9**, 295 (1996).

[21] R. Courant, K. Friedrichs, and H. Lewy, On the partial difference equations of mathematical physics, IBM J. Res. Dev. **11**, 215 (1967).

[22] K. Rothemund, H. W. Glock, M. Borecky, and U. van Rienen, Eigenmode calculation in long and complex rf structures using the coupled S-parameter calculation technique, in *Proceedings of the 6th International Computational Accelerator Physics Conference, ICAP2000* (2000), https://flash.desy.de/sites2009/site_vuvfel/content/e403/e1644/e1446/e1448/infoboxContent1684/TESLA2000-33.pdf.

[23] K. Rothemund, H. W. Glock, and U. van Rienen, Eigenmode calculation of complex rf-structures using S-parameters, in IEEE Trans. Magn. **36**, 1501 (2000).

[24] H. W. Glock, K. Rothemund, and U. van Rienen, CSC—A procedure for coupled S-parameter calculations, IEEE Trans. Magn. **38**, 1173 (2002).

[25] T. Flisgen, Compact state-space models for complex superconducting radio-frequency structures based on model order reduction and concatenation methods, Ph.D. thesis, Universität Rostock, 2015.

[26] T. Flisgen, J. Heller, T. Galek, L. Shi, N. Joshi, N. Baboi, R. M. Jones, and U. van Rienen, Eigenmode compendium of the third harmonic module of the European x-ray free electron laser, Phys. Rev. Accel. Beams **20**, 042002 (2017).

[27] T. Flisgen, A. Vélez, J. Heller, S. G. Zadeh, and U. van Rienen, Computation of eigenmodes in the BESSY VSR cavity chain by means of concatenation strategies, in *Proceedings of the 13th International Computational Accelerator Physics Conference, ICAP2018, Key West, FL, 2018* (JACoW, Geneva, Switzerland, 2019), pp. 253–259.

[28] T. Flisgen, E. Gjonaj, H.-W. Glock, and A. Tsakanian, Generalization of coupled *S*-parameter calculation to compute beam impedances in particle accelerators, Phys. Rev. Accel. Beams **23**, 034601 (2020).

[29] E. Shaposhnikova, E. Ciapala, and E. Montesinos, Upgrade of the 200 MHz rf system in the CERN SPS, in *Proceedings of the 2nd International Conference, IPAC-*

2011, San Sebastian, Spain (2011), pp. 214–216, https://accelconf.web.cern.ch/IPAC2011/papers/mopc058.pdf.

[30] G. Dome, The SPS acceleration system: Travelling wave drift-tube structure for the CERN SPS, in *Proceedings of the 1976 Proton Linear Accelerator Conference, Chalk River, Ontario, Canada* (CERN, Geneva, Switzerland, 1976), pp. 138–147.

[31] P. Kramer and C. Vollinger, Measurement of rf voltage in long traveling wave accelerating structures with application to the CERN Super Proton Synchrotron, Phys. Rev. Accel. Beams **22**, 101002 (2019).

[32] A. Hanif Halim and I. Ismail, Combinatorial optimization: Comparison of heuristic algorithms in travelling salesman problem, Arch. Comput. Methods Eng. **26**, 367 (2019).

[33] MATLAB, version 9.6.0 (R2019a) Natick, Massachussets: The MathWorks Inc. 2019, https://mathworks.com/.

[34] E. Gjonaj, W. Ackermann, T. Lau, T.Weiland, and M. Dohlus, Coupler kicks in the third harmonic module for the XFEL, in *Proceedings of the 23rd Particle Accelerator Conference, Vancouver, Canada, 2009* (IEEE, Piscataway, NJ, 2009).

[35] https://www.salome-platform.org/.